Journal of Power Sources 199 (2012) 174–178

Contents lists available at SciVerse ScienceDirect

Journal of Power Sources

journal homepage: www.elsevier.com/locate/jpowsour

Short communication

Agglomeration behavior of nickel particles on YSZ and TiO_2-doped YSZ electrolytes

Haruo Kishimoto[a,*], Akihito Suzuki[b], Taro Shimonosono[a], Manuel E. Brito[a], Katsuhiko Yamaji[a], Teruhisa Horita[a], Fumio Munakata[b], Harumi Yokokawa[a]

[a] National Institute of Advanced Industrial Science and Technology (AIST), AIST Central No. 5, Higashi 1-1-1, Tsukuba, Ibaraki 305-8565, Japan
[b] Tokyo City University, 8-15-1 Todoroki, Setagaya-ku, Tokyo 158-0082, Japan

ARTICLE INFO

Article history:
Received 2 August 2011
Received in revised form
22 September 2011
Accepted 13 October 2011
Available online 20 October 2011

Keywords:
Solid oxide fuel cell (SOFC)
Nickel agglomeration
Anode
Scanning electron microscope (SEM)
Scanning probe microscope (SPM)

ABSTRACT

Agglomeration behavior of nickel thin films on the yttria stabilized zirconia (YSZ) and TiO_2 doped-YSZ electrolytes under a reducing condition and at solid oxide fuel cell (SOFC) operating temperatures was investigated by scanning electron microscopy (SEM) and scanning probe microscopy (SPM) to clarify whether this method is appropriate to investigate fundamental physicochemical properties that determine the microstructure of nickel/zirconia cermet anodes. Nickel agglomeration is enhanced with increasing annealing temperature and with decreasing the thickness of nickel films. Nickel agglomeration behavior was found to be essentially the same between YSZ and TiO_2-doped YSZ electrolytes, forming small nickel particles with average diameter of less than 550 nm. Nonetheless, the effect by TiO_2 doping to YSZ appeared for larger nickel particles formed due to enhancement in wettability of nickel metal on the electrolyte. It is demonstrated that the present method is actually an useful and powerful tool to investigate fundamental physicochemical properties in metal/oxide systems.

1. Introduction

In solid oxide fuel cells (SOFCs), composite porous materials consisting of nickel metal and oxide ceramic, so called *cermet*, have generally been used as anode materials. While improvement is seen in many other degradation phenomena, agglomeration of nickel particles in the anode remains as one of the important problems to establish the long-time durability even for intermediate temperature SOFC systems [1–3]. Morphology change in the anode, especially reduction of the gas–nickel–oxide triple phase boundaries (TPBs) and isolation of the nickel network, reduces the anode performance and, as a result, it leads to decrease of durability and reliability of SOFC systems. Nickel agglomeration is induced by factors like long time operation at high temperature [4–9], impurities in the fuel (i.e., sulfur and phosphorus) [10–16] and so on so forth.

To avoid or to control the nickel agglomeration in the anode, several approaches have been investigated. One is to control the morphology of nickel cermet anode [17,18]. Another is to modify the oxide component in the anode. It was reported that TiO_2 doping into the yttria stabilized zirconia (YSZ) is effective in reducing the agglomeration of nickel particles [19] in addition to enhance electron conductivity in the reducing atmosphere [20–23].

The microstructure of nickel cermet anode is rather complex because the networks of nickel, oxide and pore are three-dimensionally connected to maintain the electron path, the mechanical strength and the gas diffusion, respectively, with high density of TPBs. It is therefore quite difficult to analyze and compare the microstructure among various real cermet anodes. Our group has developed a simple method for analyzing gas/nickel/oxide substrate interactions taking advantage of the agglomeration behavior of nickel thin films on oxide substrates under a controlled condition [24,25]; a similar technique was recently reported by Baumann et al. using platinum (Pt) electrode on a YSZ electrolyte [26]. In this study, nickel agglomeration behavior on YSZ electrolyte is examined under a reducing atmosphere at SOFC operating temperatures between 773 K and 1173 K to validate this experimental method as an evaluation method for "wettability" of nickel on oxides. In the present investigation, this analysis method is applied to both YSZ electrolyte and TiO_2-doped YSZ electrolyte. The TiO_2 doping effect on the nickel agglomeration behavior is evaluated and compared with data reported by Skarmoutsos et al. [19].

2. Experimental

Nickel thin film was sputtered on stabilized zirconia substrates. Cubic stabilized zirconia with 8 mol% Y_2O_3 (8YSZ) and 5 mol% TiO_2

* Corresponding author. Tel.: +81 29 861 4542; fax: +81 29 861 4540.
E-mail address: haruo-kishimoto@aist.go.jp (H. Kishimoto).

0378-7753/$ – see front matter © 2011 Elsevier B.V. All rights reserved.
doi:10.1016/j.jpowsour.2011.10.047

doped 8YSZ (Ti-8YSZ) were used as substrate materials. Powders of 8YSZ (TZ-8Y, Tosoh Co., Japan) and a mixture of TiO_2 (99.9% purity, Wako Pure Chemical Industries, Ltd., Japan) and 8YSZ powders were shaped into disks and pressed by cold isostatic press (CIP) at 390 MPa for 5 min. Pressed disks were sintered at 1673 K for 5 h in air. The surface of sintered disks was polished by diamond slurry of 1 μm. Crystal structure of sintered substrates was identified by powder X-ray diffraction (XRD, RINT-Ultima III, Rigaku Co., Japan): Both, 8YSZ and Ti-8YSZ, were identified as the cubic single phase. Nickel thin films were deposited on the polished surface of substrate materials by RF sputtering method. Sputtering condition is under 2 Pa of argon gas atmosphere without substrate heating. Thickness of nickel film was varied from several 10 nm to sub-μm level by changing sputtering time. The thickness was measured by scanning electron microscope (SEM, VE-7800, KEYENCE Co., Japan) in the cross-section observation of sputtered samples. The samples were annealed under a reducing condition of 1% humidified argon (Ar) balanced 50 vol% of H_2 mixture gas for 2 h at temperatures between 773 K and 1173 K. The microstructure of the nickel film and the three-dimensional structure of agglomerated nickel particles were analyzed by SEM and scanning probe microscope (SPM, SPA-3000HV, Seiko Instruments Inc., Japan), respectively.

3. Results and discussion

Microstructures of the dewetted nickel films on the YSZ substrate after annealing are shown in Fig. 1. The dewetting pattern was apparently determined in terms of the experimental conditions given by the annealing temperature and the film thickness. These patterns can be categorized into three stages. (I) Significant nickel agglomeration was not observed in Fig. 1a, b, d, e and g. Those samples are annealed at 773 K and at 973 K with a rather thick film. In this stage, some grooves were observed on the nickel surface. Nickel migration took place to form pores which penetrate to the oxide substrate. (II) Then net-shape structure was observed in Fig. 1c, h and j. Those samples are annealed at 1173 K with 540 nm thickness, at 973 K with 180 nm thickness and at 773 K with 80 nm thickness, respectively. (III) Isolated particles were observed with thinner films especially annealed at 1173 K. For 80 nm film, many rounded and isolated particles were obtained. Those changes in microstructure of dewetted nickel film are due to annealing temperature as well as film thickness. Agglomeration was suppressed at lower temperatures and thicker nickel films. This strongly suggests that those changes are governed by a thermally activated processes. The most plausible process should be diffusion; without diffusion, any change in morphology could not occur. To examine this idea, analysis was made by using the following fundamental equation concerning diffusion distance, x, and diffusion time, t;

$$Dt \approx x^2 \tag{1}$$

where D is the self diffusion coefficient of nickel. Using this relationship, the thickness of the nickel film can be converted to some quantities to be compared with diffusion properties;

$$D(\text{equivalent}) = \frac{h^2}{t_{\text{exp}}} \tag{2}$$

where h is the thickness of the nickel film and t_{exp} is the holding time in the present investigation, namely 3600 s. In Fig. 2, the

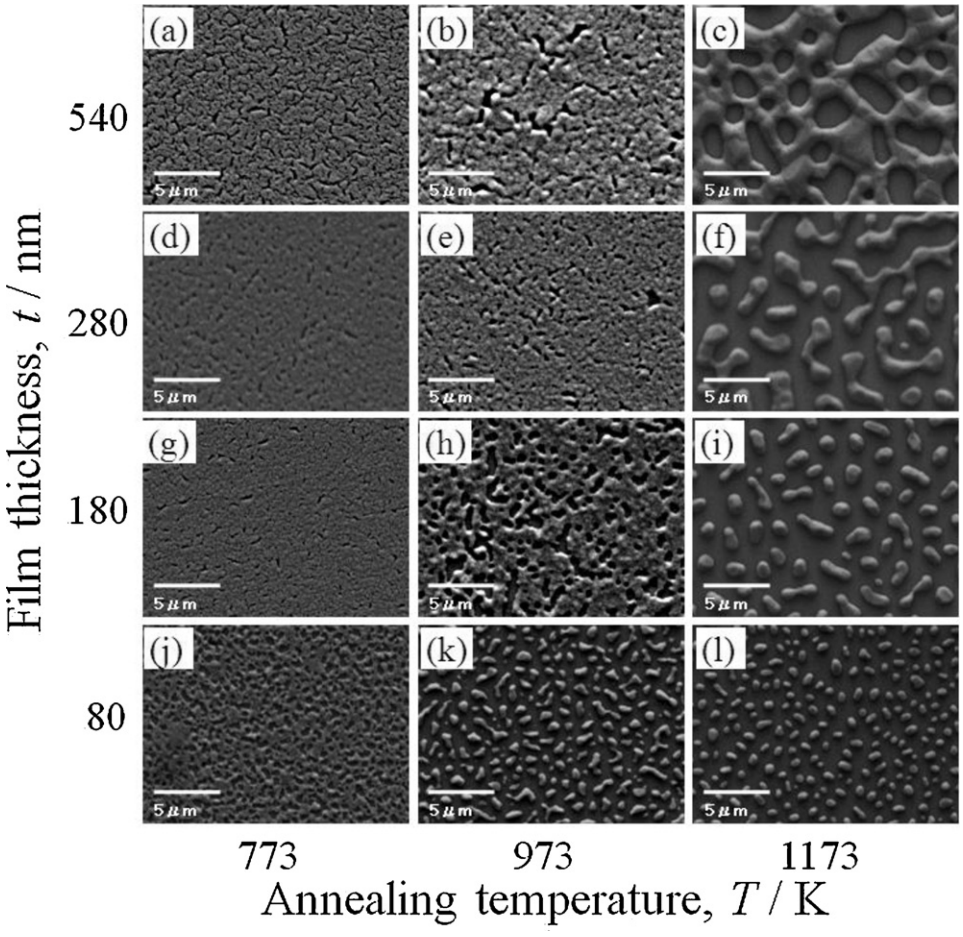

Fig. 1. SEM images of the surface for the annealed nickel thin film on the 8YSZ substrate.

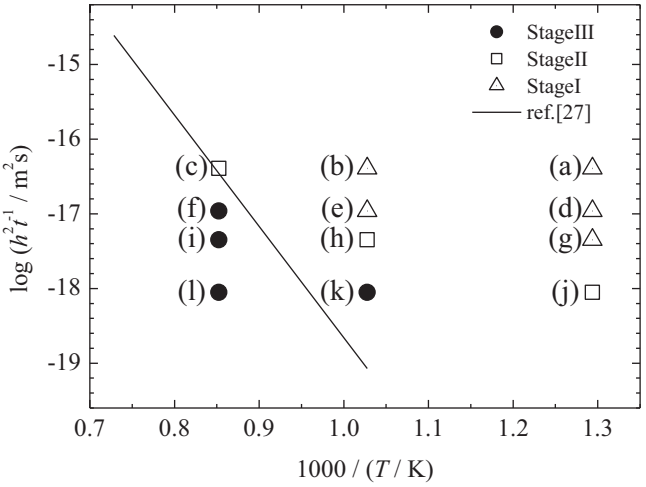

Fig. 2. Relationship between annealing temperature and calculated diffusion coefficient for the present results. Diffusion coefficient is calculated from Eqs. (1) and (2). The reaction stages are plotted as symbols of open triangles for stage I, open squares for stage II, and closed circles for stage III.

present results of the reaction stages are plotted as symbols (triangles for stage I, squares for stage II, and closed circles for stage III). Reported nickel self diffusion coefficient data were also plotted in the same figure [27]. The borderline between stage II and stage III is essentially the same as reported diffusion coefficients. Note however that point (*k*) in Fig. 2 slightly deviated from the stage III area estimated from the above relation using self diffusion coefficient data. This point is for the thin film at a lower temperature as 973 K. For smaller particles, surface area is large relatively to volume. In general, mass transport on the surface (surface diffusion) is faster than in bulk especially at low temperatures. Therefore, for smaller particles, the apparent diffusion rate can be enhanced and this could provide an explanation for deviation from the estimated area. Despite this deviation, the fundamental rate determining process for nickel agglomeration on the YSZ surface can be ascribed essentially to the Arrhenius-type bulk diffusion of nickel.

To analyze the agglomeration behavior in more details, nickel particles obtained by annealing of 60 nm thick film at 1173 K for 2 h were used because a large number of rounded and isolated particles were available. Wettability analysis method was adopted for solid-state agglomerated nickel particles on the solid substrates on a trial basis. The apparent contact angle, θ, was calculated from the averaged diameter, d, and the height, h, of agglomerated each particle by following equation:

$$\theta = 2\tan^{-1}\left(\frac{2h}{d}\right) \quad (3)$$

where h and d were determined from SPM analysis images for the substrates of the 8YSZ and the Ti-8YSZ as shown in Fig. 3. About 30

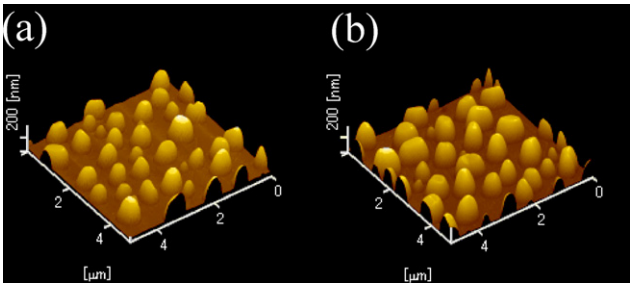

Fig. 3. SPM images of agglomerated nickel particles on the (a) 8YSZ and (b) Ti-8YSZ substrate.

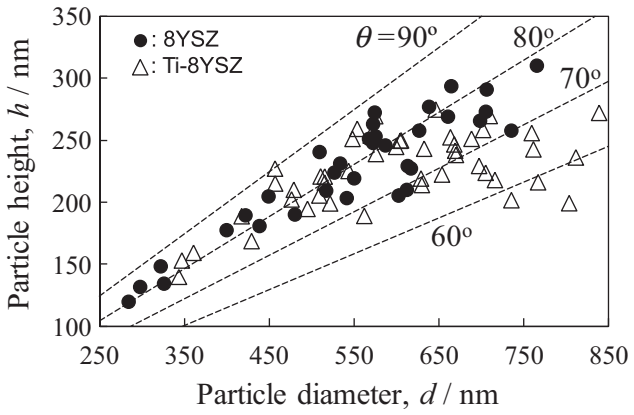

Fig. 4. Relationship between the averaged particle diameter, d, and height, h, for the the annealed nickel thin film on the 8YSZ and Ti-8YSZ substrates. Dashed lines show the same contact angle, θ, calculated from Eq. (3).

of rounded and isolated particles were observed in 5 μm × 5 μm area for both substrates. No apparent difference was distinguished between agglomerated nickel particles on the 8YSZ and those on the Ti-8YSZ. The averaged diameter, d, was obtained from the averaging of four diameters across a particle and the particle height was adopted as the maximum height in a particle. Fig. 4 shows the relationship between the averaged particle diameter, d, and the maximum height, h, for the agglomerated nickel particles on the 8YSZ and the Ti-8YSZ substrates. For the 8YSZ substrate, the particle height linearly increased with increasing particle diameter. The contact angle, θ, was about 80° for all particles. In this sense, agglomeration behavior was almost uniform in the particle size from 250 nm to 800 nm for the 8YSZ substrate. For the Ti-8YSZ substrate, agglomeration behavior is essentially the same as the 8YSZ substrate in the particle size range from 350 nm to 550 nm; that is, a TiO_2 doping effect is not apparent for smaller particle size less than 550 nm. In the larger particle size range, however, the relationship between particle diameter, d, and height, h, changes for the Ti-8YSZ substrate. The h values for the Ti-8YSZ substrate were gradually deviated from those for the 8YSZ substrate in the direction of smaller values with increasing d value more than 550 nm. This result corresponds to the fact that the apparent contact angle, θ, decreases with increasing particle size for the Ti-8YSZ substrate. The apparent contact angle, θ, is about 80° for the particle with d = 550 nm and it becomes about 60° for the particles with d = 800 nm. The effect of TiO_2 doping into the 8YSZ electrolyte reduces the contact angle, i.e. improving the wettability of nickel metal on the electrolyte, and this effect appears only for nickel particles larger than d = 550 nm.

Wettability of *melted* nickel on YSZ and TiO_2 dissolved YSZ electrolytes were already reported by Tsoga et al. [28]. The TiO_2 dissolution into 8YSZ electrolyte improves the wettability of *melted* nickel on the electrolyte. Their observed contact angle for the TiO_2 dissolved YSZ is 103°, while that for YSZ is 117° at 1500 °C. The present results for *solid* nickel on solid electrolyte confirm effects of TiO_2 doping on wettability. They measured the contact angles in the liquid state just because they wanted to know the effect of doping TiO_2 on the microstructure of those Ni–cermet anodes which will not be in liquid state during the fabrication. They actually measured the characteristic features of the cermet anodes with and without TiO_2 and also they checked the durability of those anodes. They confirmed the effect of change in wettability for the TiO_2-doping anodes [19]. From the present results of agglomeration tests in the solid-solid systems, the following important features can be derived:

(1) The present results obtained from the operation temperature range show essentially the same tendency in the wettability. This clearly indicates that the surface tension or the nickel-oxide interface energy plays an important role in determining the microstructure of the cermet anode.
(2) Because the experimental conditions can be easily selected according to the requirements for what kind of information should be obtained, the present technique can be easily applied for a wide variety of research topics. The effect of the oxide component in the cermet anode on the microstructure or on the electrochemical performance is one of such big topics. Effects of water vapors or impurities will be also important issues.
(3) In some cases, solid-like features of the nickel become important. For example, facet formation was observed. This should be related with solid–gas interactions or enhanced surface diffusion and their relation to the change in surface energy or surface morphology. The present method seems quite useful for such purpose, too.

Theoretically, the contact angle, θ, for nickel particle on the flatten oxide is calculated by Young's law:

$$\gamma_{YSZ} = \gamma_{Ni}\cos\theta + \gamma_{Ni/YSZ} \quad (4)$$

where γ_{YSZ}, γ_{Ni} and $\gamma_{Ni/YSZ}$ are surface tensions between YSZ and gas, between nickel and gas and between nickel and YSZ, respectively. Contact angle, θ, is obtained from the balance of surface tensions. For the larger particles, in those TiO_2 doping effect is observed, γ_{YSZ} and/or $\gamma_{Ni/YSZ}$ can be affected by TiO_2 doping in the 8YSZ, while γ_{Ni} can be regarded as unchanged on TiO_2 doping. Because θ decreases with TiO_2 doping, TiO_2 doping leads to increases in γ_{YSZ} and/or decreases in $\gamma_{Ni/YSZ}$. Titanium ions in TiO_2 doped YSZ can be reduced from tetravalent to trivalent states under a reducing condition:

$$2Ti_{Zr}^{x} + 4O_{o}^{x} = 2Ti_{Zr}^{\prime} + 3O_{o}^{x} + V_{o}^{\bullet\bullet} \quad (5)$$

As a result, the electronic conductivity increase [20–23] so that this mixed conductive nature of TiO_2 doping is expected to help the anode performance [20]. The effect of TiO_2 doping on the nickel agglomeration on YSZ should be related to these defects. Titanium trivalent ions affect the electronic structure in the YSZ lattice, and therefore some stronger interaction between nickel metal and the TiO_2 doped YSZ could be expected. According to the present results, this electronic structure change may lower $\gamma_{Ni/YSZ}$. Other effects can be expected due to the oxygen vacancy and trivalent titanium formation on the surface of YSZ. By forming these defects on the surface, adsorbate should be changed compared with pure YSZ, such as Brønsted type acid point formation. This may affect the increases in γ_{YSZ}.

The TiO_2 doping effect disappears for those smaller nickel particles in which the surface region has a large contribution to energetic, that is, the contribution of γ_{Ni} becomes predominant rather than $\gamma_{Ni/YSZ}$ for those smaller particles. Similarly to the present results, an interesting phenomenon was observed for carbon deposition behavior for the Ni/GDC system [24]; carbon deposition was observed only on small size (with less than submicrometer size) nickel particles and was suppressed on the nickel surface of larger nickel particles. For larger particles, the present results revealed that the contact angles are determined by the interface energy as well as the surface energy. In real SOFC anodes, particle/grain size is in the order of 0.5–3 μm so that some difference can be expected in the microstructure determined by various oxide components in cermet. This also implies that durability of nickel cermets may be different among the oxide components such as YSZ, ScSZ, or GDC. The present agglomeration method seems useful to identify those physicochemical properties which provide crucial effects for the durability of cermet anodes by examining the two dimensional distribution of nickels instead of complicated 3D microstructure of real anodes. Furthermore, the present method also provides a basis of examining effects of impurities such as sulfur, phosphor etc., on nickel morphology as well as effects of water vapors on anode degradation in terms of changes in microstructure.

4. Conclusion

Nickel agglomeration behavior on the 8YSZ electrolyte and the TiO_2-doped 8YSZ electrolyte has been investigated by the wettability analysis method. Nickel thin film was sputtered on oxide plate and heat-treated for a selected period of time at selected temperatures. It has been found that agglomeration of nickel thin film was enhanced at higher temperature and for the thinner nickel film. Contact angle of agglomerated nickel particles was successfully determined even for heat treatment without forming any liquid nickel. This is about 80° for the 8YSZ electrolyte at 900 °C and is substantially smaller than that determined for liquid nickel and solid oxide, namely 120° at 1500 °C. The nickel agglomerated behavior of Ti-8YSZ electrolyte is the same as that of 8YSZ for the nickel particles with the diameter less than 550 nm. For larger particles, in contrast, the contact angle of nickel particles decreased on the Ti-8YSZ electrolyte with increasing of particle diameter. The doping effect on the nickel particle agglomeration thus appears to depend on the particle size. Those results clarifies that the present agglomeration method is quite useful to investigate the fundamental physicochemical properties for the interface energy as well as the surface energy of nickel which must govern the microstructure in the long period of operation time. It is highly hoped that the present method will be applied to examine the role of the oxide component in cermet anodes or to examine impurities effects on nickel anode performance and their relation to the surface energy of nickel/surface species in the nickel surface.

Acknowledgement

A part of this study was financially supported by the New Energy and Industrial Technology Development Organization (NEDO) of Japan.

References

[1] H. Yokokawa, ECS Trans. 35 (2011) 207–216.
[2] M.H. Pihlatie, A. Kaiser, M. Mogensen, M. Chen, Solid State Ionics 189 (2011) 82–90.
[3] T. Matsui, R. Kishida, J.Y. Kim, H. Muroyama, K. Eguchi, J. Electrochem. Soc. 157 (2010) B776–B781.
[4] T. Iwata, J. Electrochem. Soc. 143 (1996) 1521–1525.
[5] A. Ioselevich, A.A. Kornyshev, W. Lehnert, J. Electrochem. Soc. 144 (1997) 3010–3019.
[6] A. Faes, A. Hessler-Wyser, D. Presvytes, C.G. Vayenas, J. Van herle, Fuel Cells 9 (2009) 841–851.
[7] D. Simwonis, F. tietz, D. Stöver, Solid State Ionics 132 (2000) 241–251.
[8] R. Vaßen, D. Simwonis, D. Stöver, J. Mater. Sci. 36 (2001) 147–151.
[9] Z. Jiao, N. Takagi, N. Shikazono, N. Kasagi, J. Power Sources 196 (2011) 1019–1029.
[10] F.N. Cayan, M. Zhi, S.R. pakalapati, I. Celik, N. Wu, R. Gemmen, J. Power Sources 185 (2008) 595–602.
[11] C.A. Coyle, O.A. Marina, E.C. Thomsen, D.J. Edwards, C.D. Cramer, G.W. Coffey, L.R. Pederson, J. Power Sources 193 (2009) 730–738.
[12] C. Xu, J.W. Zondlo, H.O. Finklea, O. Demircan, M. Gong, X.-B. Liu, J. Power Sources 193 (2009) 739–746.
[13] H. Kishimoto, Y.P. Xiong, K. Yamaji, T. Horita, N. Sakai, M.E. Brito, H. Yokokawa, J. Chem. Eng. Jpn. 40 (2007) 1178–1182.
[14] H. Kishimoto, T. Horita, K. Yamaji, M.E. Brito, Y.-P. Xiong, H. Yokokawa, J. Electrochem. Soc. 157 (2010) B802–B813.
[15] H. Kishimoto, K. Yamaji, Y.-P. Xiong, T. Horita, M.E. Brito, H. Yokokawa, ECS Trans. 17 (2009) 31–35.
[16] D.G. Ivey, E. Brightman, N. Brandon, J. Power Sources 195 (2010) 6301–6311.
[17] M. Watanabe, H. uchida, M. Shibata, N. Mochizuki, K. Amikura, J. Electrochem. Soc. 141 (1994) 342–346.
[18] H. Itoh, T. Yamamoto, M. Mori, T. Horita, N. Sakai, H. Yokokawa, M. Dokiya, J. Electrochem. Soc. 144 (1997) 641–646.

[19] D. Skarmoutsos, A. Tsoga, A. Naoumidis, N. Nikolopoulos, Solid State Ionics 135 (2009) 439–444.
[20] W.L. Worrell, Electrochemical Society Proceedings, 2001-28, 2001, pp. 75–89.
[21] K. Kobayashi, S. Yamaguchi, T. Higuchi, S. Shin, Y. iguchi, Solid State Ionics 135 (2000) 643–651.
[22] M. Mori, Y. Hiei, H. Itoh, G.A. Tompsett, N.M. Sammes, Solid State Ionics 160 (2003) 1–14.
[23] X. Mantzouris, N. Zouvelou, V.A.C. Haanappel, F. Tietz, P. Nikolopoulos, J. Mater. Sci. 42 (2007) 10152–10159.
[24] M. Yoshinaga, H. Kishimoto, M.E. Brito, K. Yamaji, T. Horita, H. Yokokawa, J. Ceram. Soc. Jpn. 119 (2011) 307–309.
[25] M. Yoshinaga, H. Kishimoto, K. Yamaji, Y.-P. Xiong, M.E. Brito, T. Horita, H. Yokokawa, Solid State Ionics 192 (2011) 571–575.
[26] N. Baumann, E. Mutoro, J. Janke, Solid State Ionics 181 (2010) 7–15.
[27] K. Hirano, R.P. Agarwala, B.L. Averback, M. Cohen, J. Appl. Phys. 33 (1962) 3049–3054, from Diffusion database (Kakusan). Available from: http://diffusion.nims.go.jp/diffusion/frame_top_jp (accessed 13.07.11).
[28] A. Tsoga, A. Naoumidis, N. Nikolopoulos, Acta Mater. 44 (1996) 3679–3692.